A New Model for Fatigue Threshold

A. Sengupta and S.K. Putatunda[1]

Department of Materials Science and Engineering,
Wayne State University,
Detroit, Michigan 48202, USA

CONTENTS

[1] To whom all correspondence should be addressed.

ABSTRACT

A new model for fatigue threshold is proposed. The model takes into consideration the influence of material strength, grain size, and load ratio on fatigue threshold. Fatigue crack growth behavior of a solid solution strengthened nickel-based superalloy (Incoloy 825) was investigated to examine the applicability of this model. The investigation also examined the influence of heat treatment on the resultant microstructures and the near threshold fatigue crack growth behavior of this alloy.

Compact tension specimens with transverse-longitudinal (TL) orientation were prepared from Incoloy 825 and heat treated in four different ways to produce four different microstructures (grain sizes). Fatigue crack growth behavior of these materials as well as the as-received material (without heat treatment) was studied in room temperature ambient atmosphere.

The results of the present investigation demonstrate that the fatigue threshold of the material increases with increase in grain size of the material. The fatigue threshold values predicted by the model were in good agreement with the experimentally determined values.

1. INTRODUCTION

The fatigue crack growth rate, da/dN, has been related to the stress intensity range, ΔK, and the Paris equation /1/ has been found to be extremely useful in characterizing the fatigue crack growth rate. The Paris equation relates the crack growth rate, da/dN, with the stress intensity range, ΔK, in the form of a power law:

$$\frac{da}{dN} = C \cdot (\Delta K)^m$$

where C and m are material constants and $\Delta K = K_{max} - K_{min}$ = the difference between maximum and minimum stress intensity factors. However, when the experimental crack growth data is plotted in terms of log da/dN versus log ΔK, it often shows a sigmoidal curve with varying slopes (see Fig. 1) instead of a single straight line as one would expect from such a plot. There are three distinct regions in such a plot. In region I or the slow crack growth region, the crack growth rate is very slow and deviates from the Paris equation. This region is also called the threshold region. In region II or the linear region, the crack growth rates increase linearly with ΔK and the Paris equation is usually obeyed by most materials. In region III or the fast fracture region, the crack growth rate accelerates and again deviates from the Paris equation.

In addition to all these regions, there is also a threshold stress intensity factor, ΔK_{th}, below which the crack growth rate approaches a zero value. According to ASTM standard E-647 /2/, fatigue threshold is defined as the value of stress intensity factor at which the crack growth rate is of the order of 10^{-10} m/cycle.

The threshold region is very important since a significant portion of the life of the structural components is spent in this region. The threshold stress intensity factor, ΔK_{th}, is also a very important parameter for structural design since the structural components designed on the basis of fatigue threshold are expected to have infinite lives or at least last for a very long period of time.

Numerous variables /3-10/ are known to affect the fatigue threshold and near threshold crack growth rate. Amongst these, the influence of microstructural parameters such as grain size and material strength and the load ratio (R) are significant and extremely important from a practical point of view. Both yield strength and grain size are known to have significant influence /6,7,11,12/ on fatigue threshold. Generally their effects are opposite in nature. Fatigue threshold usually decreases with increase in yield strength of the material. On the other hand, fatigue threshold usually increases with increase in grain diameter of the material. Furthermore, fatigue threshold decreases with increase in load ratio. Even though there exist several models for fatigue threshold in the literature /13-15/, a coherent model incorporating the effect of all these parameters on fatigue threshold is still lacking.

Based on the above facts, a new model for fatigue threshold has been developed by these authors. This model is presented in Section 2. The proposed model takes into consideration the effects of grain size, yield strength and load ratio on fatigue threshold. The primary objective of this investigation was to examine the

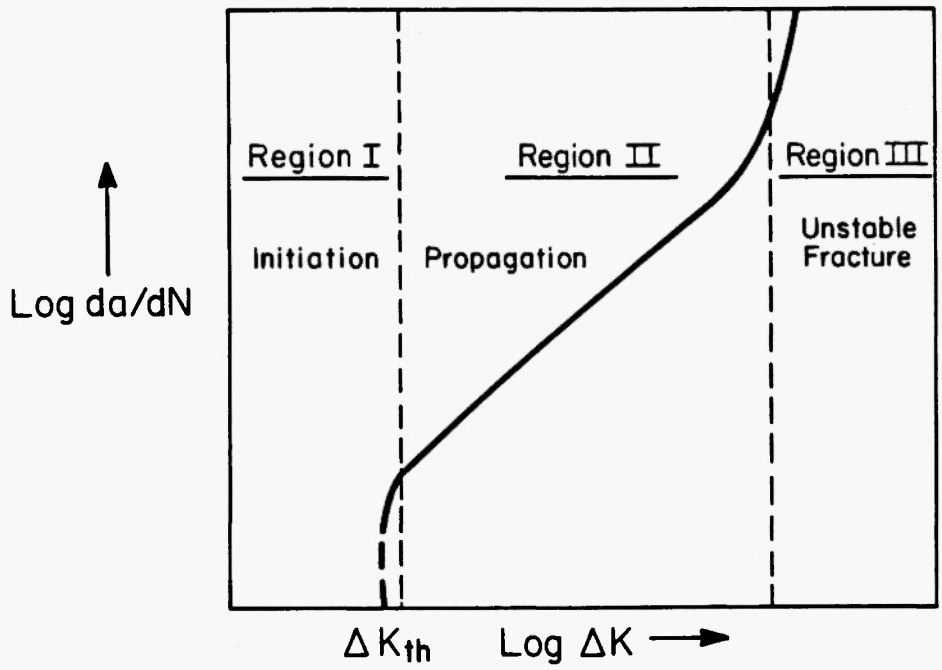

Fig. 1: Schematic representation of fatigue crack growth data according to Paris equation.

applicability of this model in Incoloy 825.

Incoloy 825 is a solid solution strengthened nickel based superalloy. This material is used extensively in many high temperature applications such as piping material in steam boilers, super heater tubes in solid waste burners, expansion joints, lining material in bag house scrubbers, etc. Fatigue crack growth data of this material is important and needed for the safe life prediction of these components. Moreover, earlier studies /16,17/ by these authors have shown that it is possible to vary the grain size of this material by suitable heat treatments (by solution treatment after prior cold working). This makes it an ideal material for verification of the proposed model.

2. MODEL FOR FATIGUE THRESHOLD

The following assumptions were made in developing the model:

(a) During fatigue loading, the material ahead of the crack tip undergoes plastic deformation and a plastic zone forms ahead of the crack tip.

During the loading part of the cycle the material ahead of the crack tip undergoes tensile loading whereas in the unloading part of the fatigue cycle the material ahead of the crack tip undergoes compressive loading. This tensile loading during the loading part of the cycle and compressive loading during the unloading part of the cycle causes either cyclic hardening or softening /18/ of the material. As a result of this cyclic hardening or softening, the local yield strength of the material at the crack tip region will be different from its monotonic yield strength.

(b) A plastic zone forms corresponding to maximum stress intensity factor in the loading cycle. The plastic zone size formed ahead of the crack tip during the fatigue cycling can be expressed using Von Misces criteria /19/ as follows:

$$Rp = \frac{K_{max}^{2}{}_{,th}}{2\pi(m\cdot\sigma'_{ys})} \cos^2\frac{\theta}{2}\left[1 + 3\sin^2\frac{\theta}{2}\right] \qquad (1)$$

where

$K_{max,_{th}}$ = maximum stress intensity factor corres-

ponding to fatigue cycle at threshold level,

Rp = radius of the plastic zone,

σ'_{ys} = cyclic yield strength of the material,

m = constraint factor whose value depends in state of stress of the material.

The area of the plastic zone, A_p, is, therefore, given by

$$A_p = \frac{1}{2} \int_0^{2\pi} R_p^2 \, d\theta. \tag{2}$$

The area of the plastic zone as shown in the above function can be calculated with the help of the residue theorem as follows:

$$\text{Area} = \frac{i}{2} \int_0^{2\pi} R_p^2 \, d\theta$$

$$= \frac{1}{2} \left[\frac{K_{max}{}^2{}_{,th}}{2\pi (m\sigma'_{ys})^2} \right]^2 \int_0^{2\pi} \tag{3}$$

$$(\cos^4 \frac{\theta}{2} + 6\cos^4 \frac{\theta}{2} \sin^2 \frac{\theta}{2} + 9\cos^4 \frac{\theta}{2} \sin^4 \frac{\theta}{2}) \, d\theta$$

in this case

$$\int_0^{2\pi} \sin\theta d\theta = \int \frac{(z-\frac{1}{2})}{2i} \frac{dz}{iz} \tag{4}$$

and

$$\int_0^{2\pi} \cos\theta d\theta = \int \frac{(z-\frac{1}{2})}{2} \frac{dz}{iz}. \tag{5}$$

According to the residue theorem, if z_o is m_{th} order pole of the f(z) then residue $R(z_o)$ is

$$R(z_o) = \frac{1}{(m-1)!} \cdot 1m \frac{d^m}{dz^m} [(z \cdot z_o)^m f(z)] \tag{6}$$

and

$$\int f(z)dz = 2\pi i \, R(z_o) \tag{7}$$

Therefore, the area of the plastic zone, A_p, can be determined as

$$A_p = \frac{1}{2} \left[\frac{(K_{max,th})^2}{2\pi (m\sigma'_{ys}} \right]^2 [2\pi i (\frac{1}{4i} - \frac{6}{i} \frac{1}{64} + \frac{9}{i} \frac{1}{2^8}] \tag{8}$$

$$= \frac{49}{1024\pi} \left[\frac{K_{max,th}}{(m\sigma'_{ys})^4} \right] \tag{9}$$

2.1 Relationship Between Grain Size and Cyclic Plastic Zone

We assume that a source of dislocation S exists at the center of a grain and this source inside the grain will generate dislocations. During cyclic loading, this dislocation source S continues to emit dislocations. These dislocations move on intersecting slip planes and are blocked by grain boundary. The cyclic plastic zone is produced by dislocation motion and hence will be confined to these slip planes. Now, the piled up dislocation will exert back stress /20/ on the dislocation source and the dislocation emission will cease when this back stress exerted by these dislocations equals the effective shear stress, i.e. $\tau_{eff} = \tau_{applied} - \tau_i$ (where τ_i = Pierls Nabarro stress of the material), acting on the dislocation source 'S'.

At theshold level a condition such as those described is achieved and the applied stress being sufficiently low, the dislocations are unable to break through grain boundary. Hence, one can conclude that, at threshold level, the size of this cyclic plastic zone (area) will be equivalent to the area covered by the intersecting slip planes, along which the dislocations move. This is shown schematically in Fig. 2.

Area of plastic zone = area of the circle with diameter approximately equal to L.

$\therefore$ Now the area of circle with diameter L

$$A_p = \frac{\pi \cdot L^2}{4} \tag{10}$$

$$\text{Since } L \approx \frac{D}{2}, \text{ where D = grain diameter} \tag{11}$$

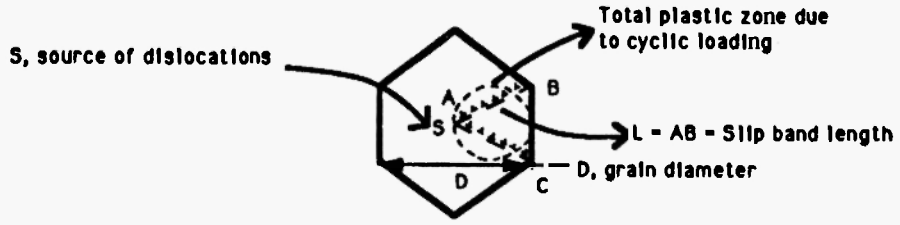

Fig. 2: Distribution of dislocations during fatigue cycle.

$$\text{Area } A_p = \frac{\pi}{4}\left(\frac{D}{2}\right)^2 \tag{12}$$

$$\therefore \text{ Area of plastic zone} = A_p = \frac{\pi D^2}{16} \tag{13}$$

As mentioned earlier, the area of the cyclic plastic zone equals the area of circle ABC at threshold level

$$\therefore \frac{49}{1024\pi}\left(\frac{K_{max,th}^4}{(m\sigma'_{ys})^4}\right) = \frac{\pi D^2}{16} \tag{14}$$

$$\therefore (K_{max,th})^4 = \frac{1024\pi}{49}\cdot\frac{\pi D^2}{16}\cdot(m\sigma'_{ys})^4 \tag{15}$$

$$\therefore K_{max,th} = \sqrt[4]{\frac{1024\pi^2}{49\cdot 16}}\; m\cdot\sigma'_{ys}\sqrt{D}. \tag{16}$$

Since ΔK is relatively low at threshold level, the ratio of the plastic zone and thickness is very small. Hence, one can assume that the plane strain condition exists at the crack tip region at threshold level. In that case, m can be approximated as $\sqrt{3}$ /21/. Putting this value of m in the above equation we get:

$$K_{max,th} = \sqrt[4]{\frac{1024\pi^2}{784}}\cdot\sqrt{3}\cdot\sigma'_{ys}\sqrt{D}. \tag{17}$$

The above equation becomes

$$K_{max,th} = 3\cdot 28\,(\sigma'_{ys})\sqrt{D} \tag{18}$$

Now at threshold level

$$\Delta K_{th} = K_{max,th} - K_{min,th}. \tag{19}$$

but load ratio R is given by:

$$R = \frac{K_{min,th}}{K_{max,th}} \tag{20}$$

$$\therefore \Delta K_{th} = K_{max,th} - R\cdot K_{max,th}. \tag{21}$$

$$= K_{max,th}(1 - R) \tag{22}$$

$$\therefore K_{max,th} = \frac{\Delta K_{th}}{1 - R}. \tag{23}$$

Putting this value of $K_{max,th}$ in Eq. 18 we get

$$\Delta K_{th} = 3\cdot 28\,\sigma'_{ys}\sqrt{D}\,(1 - R) \tag{24}$$

2.2 Some Comments About the Model

(a) The model predicts that the threshold will depend on the cyclic yield strength of the material, and hence materials that cyclically harden will have a higher fatigue threshold compared to materials that cyclically soften. Since initially hard and strong material usually cyclically soften /18/, the present model predicts a lower fatigue threshold for these materials. Similarly, the model also predicts a higher fatigue threshold value for initially soft and ductile materials which generally cyclically harden /18/. Thus, the model can explain why the influence of yield strength on fatigue threshold is different /22-25/ in different materials. The present model

can also explain the anomalies of the effect of yield strength on fatigue threshold observed in the literature, since, in some cases, higher monotonic yield strength is known to cause a decrease /22,23/ in fatigue threshold and, in other cases, higher monotonic yield strength is known to cause an increase /24,25/ in fatigue threshold.

(b) The model predicts that the normalized value of fatigue threshold with respect to cyclic yield strength is a function of $\sqrt{D}$. This is in agreement with the results reported in literatures /26,27/.

(c) Crack closure /28/ effect was not taken into consideration in the model. Hence, the model is applicable for closure free threshold only, i.e., for intrinsic fatigue threshold. Thus, the present model is applicable where no significant plasticity or roughness-induced /29/ or oxidation-induced /30/ crack closure occurs. Since in most cases, $K_{closure}$ or closure stress intensity is within 10-15% fatigue threshold, the model is still capable for predicting fatigue threshold in most materials within ± 15%.

3. EXPERIMENTAL PROCEDURE

3.1 Material

The material used in this investigation was Incoloy 825. The material was in the form of a cold rolled plate with identifiable rolling direction from Huntington Alloys, Inc. The chemical composition of the material in weight percentage is reported in Table 1.

TABLE 1
Chemical Composition of the Incoloy 825 Material in Weight %

Cr	20.2
Al	0.2
Ti	1.10
Mo	2.8
Cu	2.1
Fe	23.5
Ni	Balance
Mn	0.85
S	0.02
C	0.046

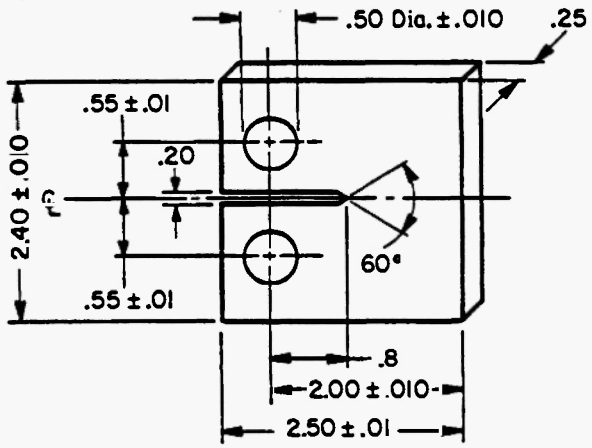

Fig. 3: Compact tension specimen (2T). Scale: full size; all dimensions in inches

3.2 Specimen Preparation

Compact tension specimens with 2T geometry in Transverse-Longitudinal (TL) orientation were prepared from the as-received cold rolled plate as per ASTM Standard E-647 /2/. A schematic of the specimens used in this study is shown in Fig. 3. The initial aspect ratio was kept as $\frac{a}{W} \approx 0.40$. After fabrication, the specimens were subjected to four different heat treatments. These heat-treated conditions are identified as B, C, D and E, while the as-received material (without heat treatment) is identified as A. All subsequent reference to the specimens in the text are based on these letter designations. Details of the heat treatment procedures and the resulting average grain diameters are reported in Table 2. The mechanical properties of the materials before and after heat treatments are listed in Table 3.

3.3 Fatigue Testing

After heat treatment, the specimens were ground on both surfaces and subsequently polished with 600 grit emery paper. This was found very helpful in locating the crack tip during fatigue testing. All these specimens were initially pre-cracked in fatigue at a ΔK level of ΔK

TABLE 2
Heat Treatment Procedures

Specimen Identification	Heat Treatment	Average Grain Diameter (μm)
A	As-received	70
B	Solution-treated at 1200 °C for 1/2 hour	106
C	Solution-treated at 1200 °C for 4 hours	175
D	Solution-heated at 1200 °C for 1/2 hour and then aged at 600 °C for 118 hours	205
E	Solution-heated at 1200 °C for 1/2 hour and then aged at 600 °C for 434 hours	205

TABLE 3
Mechanical Properties

Sample	Condition	(0.2%) YS MPa	UTS MPa	% R.A.	n	Total % Elongation	Hardness (Rockwell B)
A	As-received	337	686	47	0.14	30	88
B	Solution-treated for 1/2 hour at 1200 °C	238	584	62	0.18	44	75
C	Solution-treated for 4 hours at 1200 °C	208	564	59	0.19	40	75
D	Solution-heated at 1200 °C for 1/2 hour and then aged at 600 °C for 118 hours	250	632	57	0.18	55	86
E	Solution-heated at 1200 °C for 1/2 hour and then aged at 600 °C for 434 hours	315	745	48	0.16	55	90

n = strain hardening exponent

= 15 MPa$\sqrt{m}$ to produce a 2mm long sharp crack front. After precracking, the fatigue testing was carried out in a servohydraulic MTS test machine using the load-control mode. All tests were carried out at room temperature in ambient atmosphere using tension-tension mode. A constant amplitude sinusoidal wave form was applied and the fatigue testing was carried out at two different load ratios (R) such as R = 0.10 and R = 0.50, respectively. The crack lengths were monitored continuously with the help of an optical travelling microscope. The crack growth rates were determined according to ASTM Standard E-647 /2/. Three to four identical specimens were tested at each load ratio from each heat treated condition and fatigue crack growth rate was determined by averaging the test results from all these samples. The fatigue threshold was determined using the load shedding technique of the ASTM Standard E-647 and threshold was identified graphically by plotting log $\frac{da}{dN}$ versus log ΔK. The threshold was identified as the value of ΔK at which the crack growth rate was of the order of 10^{-10} m/cycle.

3.4 Cyclic Yield Strength

The cyclic yield strength of the materials was determined using three to four identical cylindrical specimens and obtaining their cyclically stabilized stress-strain data. From these stabilized data, the cyclic stress-strain curve was obtained. From this cyclic stress-strain curve, cyclic yield strengths were determined using the 0.2% offset value. These values are reported in Table 4.

4. RESULTS AND DISCUSSION

4.1 Influence of Heat Treatment on Microstructures

The microstructure of the material in as-received condition (A) is shown in Fig. 4a. The microstructures of the materials in heat-treated conditions B, C, D and E are shown in Figs. 4b-4e, respectively. A thorough heat treatment study was initially conducted /16,17/, where the specimens were solution treated and then aged at 600 °C for various periods. This heat treatment study indicated a peak hardness condition with very high yield strength after solution treatment at 1200 °C for half hour and aging at 600 °C for 434 hours (see Fig. 5).

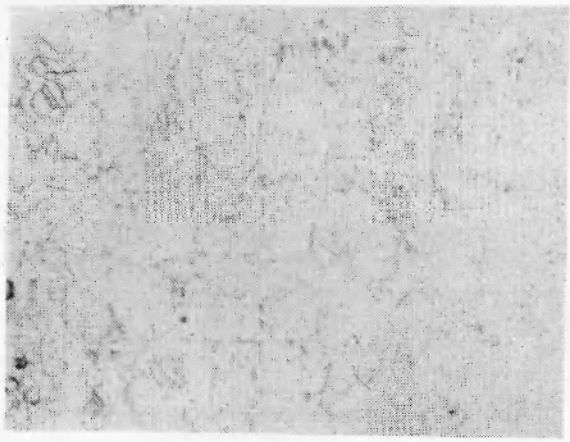

Fig. 4a: As-received (sample A) 400 .

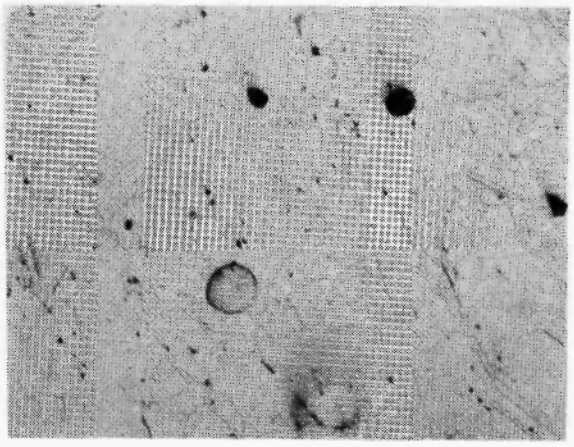

Fig. 4b: Solution treated for 1/2 hour (sample B) 400 X, Incoloy 825.

Generally, all the microstructures had an austentitic matrix with considerable amount of twins present in them. After solution treatment and aging, a gradual precipitation of carbides was observed with transmission electron microscopy (TEM). The TEM analysis further revealed:

(a) The matrix is mainly Fe,Cr and Ni.

(b) After solution treatment and aging at 600 °C, $M_{23}C_6$ type carbide precipitation occurred in heat-treated conditions D and E.

(c) In heat treated conditions of samples D and E, spherical precipitates of approximately 0.15 μm were observed. These were identified as Ti and Cr carbides. In addition, very fine γ' precipitates were observed in samples D and E /16,17/.

Microstructures

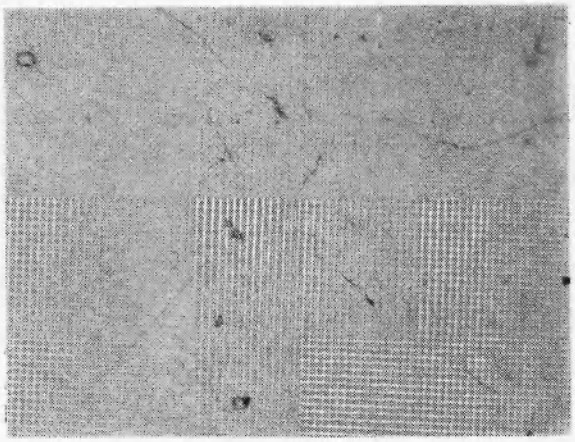

Fig. 4c: Solution treated for 4 hours (sample C) 400 X.

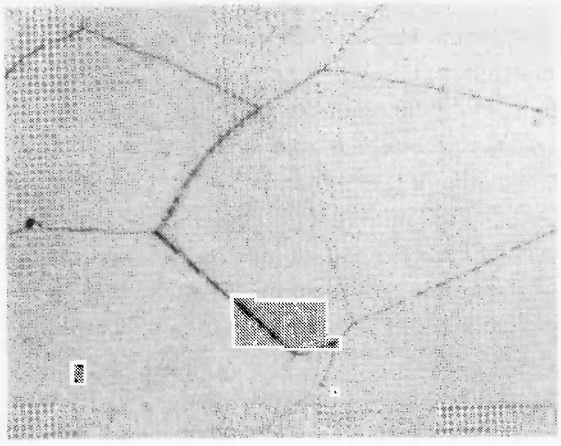

Fig. 4d: Solution treated and aged (sample D) 400 X, start of carbide precipitation after 118 hours of aging at 600 °C, Incoloy 825.

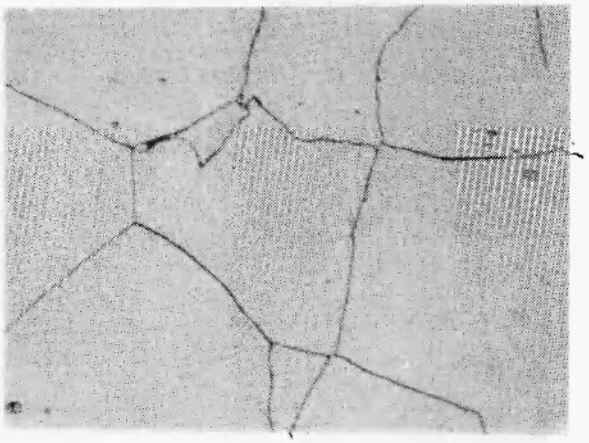

Fig. 4e: Solution treated and aged (sample E) 400 X, carbide precipitation at grain boundaries after 434 hours of aging at 600 °C, Incoloy 825.

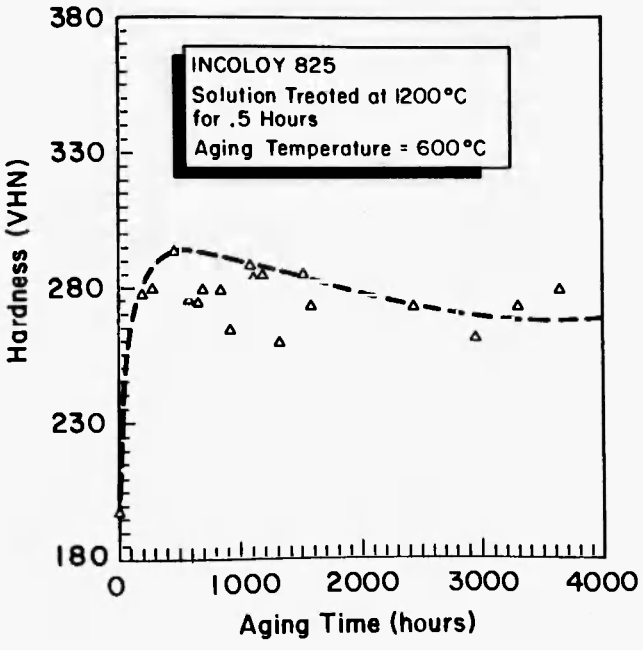

Fig. 5: Hardness versus aging time.

TABLE 4
Fatigue Threshold Values of the Material

Material Condition	Cyclic Yield Strength σ'ys (mPa)	Load Ratio R	ΔK_{th}* mPa$\sqrt{m}$	ΔK** mPa$\sqrt{m}$
A	290	0.1	6.6	7.2
		0.5	4.6	4.0
B	250	0.1	7.1	7.6
		0.5	4.9	4.3
C	280	0.1	10.5	10.8
		0.5	5.8	6.0
D	310	0.1	12.2	13.4
		0.5	11.2	7.5
E	350	0.1	14.4	14.8
		0.5	11.8	8.2

* Experimentally determined values.
** Theoretical values predicted by the model (Eq. 24).

(d) Preferential etching of the grain boundaries in sample E suggests the presence of a continuous carbide film with an average width of 2-3 μm. The transmission electron microscopy study /16,17/ further verified that these carbides reside at grain boundaries in a continuous morphology. Some earlier workers /31/ also reported a similar phenomenon occurring in nickel-based superalloys after aging at a relatively low temperature for a prolonged period of time.

(e) Hardness versus aging time relationships show (Fig. 5) that hardness of the specimens starts decreasing /16,17/ after aging beyond 434 hours.

(f) Solution treated samples B and C did not exhibit any carbide precipitation in the grain boundaries as well as in the matrix.

The formation of spherical Ti and Cr carbides together with the formation of very fine γ' precipitates in aged samples D and E increases their strength significantly. On the other hand, in solution-treated samples B and C, strength is lower due to lack of the γ' precipitates.

4.2 Validity of the Model

The experimentally determined fatigue threshold values of the material at different load ratios R = 0.1 and R = 0.5 are reported in Table 4. This table also shows the cyclic yield strength of the materials and the predicted fatigue threshold values of the material by Eq. 24. The results show that fatigue threshold of the material in heat-treated condition E is highest. Incidentally, the yield strength of the material in heat-treated condition E was highest among the heat-treated samples. Thus, our test results indicate that it is possible to increase both yield strength and fatigue threshold by a suitable heat treatment process. When comparing these data with experimentally measured values, one can observe that there is a reasonably good agreement (within ± 10%) between experimentally measured values and theoretically predicted values. The table also shows that the fatigue threshold values decrease with increase in load ratio. Furthermore, the table shows that the fatigue threshold increases with increase in grain diameters.

In Fig. 6, the theoretically predicted values are compared with the experimentally determined values, and one can see that most of the data fall around the 45° line.

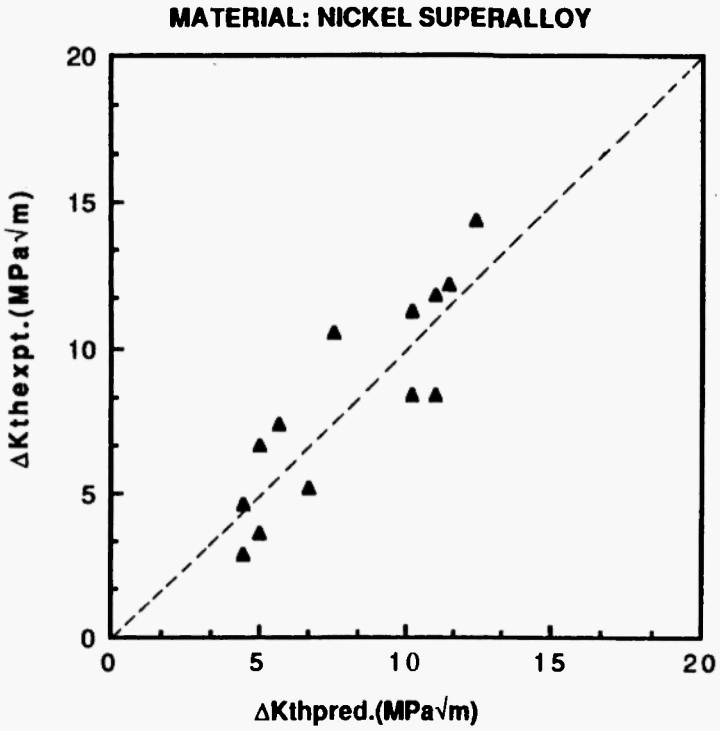

Fig. 6: Comparison of experimental fatigue threshold data with predicted fatigue threshold values.

The model is strictly valid for intrinsic fatigue threshold or closure-free fatigue threshold data. Hence, we expect a better agreement between fatigue threshold values obtained experimentally and by the theoretical model at high load ratios. However, in the present test results, there is some difference in these values at high load ratios, e.g. R = 0.5 in material D and E. The reason for this behavior is that even at very high load ratios significant amounts of roughness induced crack closure is observed /16,17/ in these materials. This is due to the fact that the crack propagated along the grain boundaries in these materials by breakage of brittle carbide film along the grain boundaries. This crack propagation along the grain boundaries in D and E material produced irregular crack trajectories. The net result is that a larger amount of surface roughness or asperities induced crack closure is produced even at very high load ratios in the materials in heat-treated conditions D and E.

The present model indicates that the fatigue threshold values decrease as the load ratio increases. It is a well-known fact /32,33/ that as the load ratio increases, fatigue threshold generally decreases. The model also predicts that at R = 0 the fatigue threshold is maximum which also is a well-known fact /34,35/. Furthermore, the present model indicates that as the grain size increases, fatigue threshold values increase. This is also in agreement with the known results in the published literature /18,19,20/.

In summary, it appears that the proposed model is a valid one and can be used to approximate the intrinsic fatigue threshold values of different materials provided cyclic yield strength, grain size, and load ratio is known.

5. CONCLUSIONS

1. A peak hardness condition was observed in Incoloy 825 after solution treatment at 1200 °C for half an hour and aging at 600 °C for 434 hours.
2. Fatigue threshold values of the material were highest in this peak aged condition.

3. The fatigue threshold values decrease with increase in load ratio.
4. Good agreement was found between experimentally measured and theoretically predicted fatigue threshold values in Incoloy 825 through the proposed model.

REFERENCES

1. Paris, P.C. and Erdogan, F., Transaction of American Society for Mechanical Engineers, *J. of Basic Eng.*, D, **85**, 528-539 (1963).
2. ASTM E-647, Annual Book of ASTM Standards, Vol. 03.01, 647-676 (1991).
3. Ritchie, R.O., *Metal Science*, **11**, 368-381 (1977).
4. Beevers, C.J., *Metal Science*, **11**, 362-367 (1977).
5. Cooke, R.J., Irving, P.E., Booth, G.S. and Beevers, C.J., *Engineering Fracture Mechanics*, **7**, 69-77 (1975).
6. Throop, J.F. and Miller, G.A., *ASTM*, Special Technical Publication, **457**, 231-244 (1970).
7. Putatunda, S.K., *Transaction of the Indian Institute of Metals*, **40** (1), 122-131 (1987).
8. Benson, J.P. and Edmonds, D.V., *Materials Science and Engineering*, **38**, 179-186 (1986).
9. Benson, J.P., *Metal Science*, **13**, 535-539 (1979).
10. Clarke, W.G. and Trout, H.E., *J. of Engineering Fracture Mechanics*, **2** (2), 223-238 (1970).
11. Ritchie, R.,O., *J. of Engineering Materials and Technology*, Transactions of ASME, **99**, 195-204 (1977).
12. Pook, L.P. and Frost, N.E., *International Journal of Fracture*, **9**, 53-58 (1973).
13. Yu, C. and Yan, M., *Fatigue of Engineering Materials and Structures*, **3**, 189-192.
14. Shadananda, K. and Shahinian, P., *International Journal of Fractures*, **13**, 585-594 (1977).
15. Taylor, D., Fatigue Threshold - a Fundamental and Engineering Application, *Engineering Materials Advisory Services*, 455-470 (1982).
16. Bartosiewicz, L., Krause, A., Spis, A., Raghavan, J. and Putatunda, S.K., International Symposium for Testing and Failure Analysis, *ISTFA 91*, 421-447 (1991).
17. Raghavan, J., Spis, A. and Putatunda, S.K., TMS Annual Meeting, Anaheim, California, February 19-24, 1990.
18. Hertberg, R.W., Deformation and Fracture Mechanics of Engineering Materials, John Wiley and Sons, 3rd Edition (1984).
19. Ewaldis, H.L., Wannell, R.J.H., Fracture Mechanics, Edward Arnold Publications (1983).
20. Taylor, D., Fatigue Thresholds, Butterworths and Co., 75-76 (1989).
21. McClintock, F.A. and Irwin, G.R., Fracture Toughness Testing and its Application, *ASTM STP*, **318**, 84-113 (1965).
22. Masounave, J. and Bailon, J.P., *Scripta Metallurgica*, **10**, 165-180 (1976).
23. Cooke, R.J. and Beevers, C.J., *Materials Science and Engineering*, **13**, 201-212 (1974).
24. Liaw, P.K. and Logsdon, W.A., *J. of Engineering and Technology*, **107**, 26-33 (1985).
25. Radon, J.C. and Woodtli, T.H., *International Journal of Fatigue*, **6**, 221-228 (1984).
26. Murakami, R. and Akizono, K., Advance Fracture Research, International Conference on Fracture 5 (ICF 5), **2**, 963-971 (1981).
27. Carlson, M.F. and Ritchie, R.O., *Scripta Metallurgica*, **1**, 113-118 (1977).
28. Bringhze, L., and Averbach, B.L., *Metallurgical Transactions*, **14A**, 1899-1906 (1983).
29. Tanaka, K., *Japan Institute of Metals*, **26**, 333-362 (1982).
30. Ritchie, R.O., *International Metals Review*, **5** and **6**, 205-250 (1989).
31. Grosshen, T.J. and McCarthy, G.P., *Metallurgical Transaction*, **16A**, 1213-1223, July 1985.
32. Barsom, J.M., *WRC Bulletin*, **194**, 33-38 (1974).

33. Klensil, M. and Lukas, P., *Materials Science and Engineering*, **9**, 231-236 (1972).

34. Weiss, V. and Lall, D., *Metallurgical Transactions*, **5A**, 1946-1963 (1974).

35. Putatunda, S.K., *Transactions of Indian Institute of Metals*, **41**, 33-36 (1989).